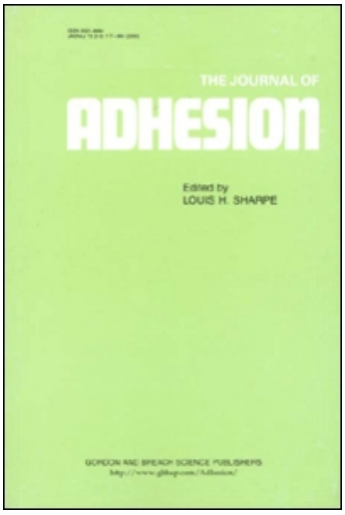

The Journal of Adhesion
Publication details, including instructions for authors and subscription information:
http://www.informaworld.com/smpp/title~content=t713453635

Adhesively Bonded Repair Proposal for Wood Members Damaged by Horizontal Shear Using Carbon-Epoxy Patches

R. D. S. G. Campilho[a]; M. F. S. F. de Moura[a]; D. A. Ramantani[a]; J. J. L. Morais[b]; A. M. J. P. Barreto[a]; J. J. M. S. Domingues[c]
[a] Departamento de Engenharia Mecânica, Faculdade de Engenharia da Universidade do Porto, Porto, Portugal [b] CITAB/UTAD, Departamento de Engenharias, Vila Real, Portugal [c] Departamento de Engenharia Mecânica, Instituto Superior de Engenharia do Porto, Porto, Portugal

Online publication date: 10 June 2010

To cite this Article Campilho, R. D. S. G. , Moura, M. F. S. F. de , Ramantani, D. A. , Morais, J. J. L. , Barreto, A. M. J. P. and Domingues, J. J. M. S.(2010) 'Adhesively Bonded Repair Proposal for Wood Members Damaged by Horizontal Shear Using Carbon-Epoxy Patches', The Journal of Adhesion, 86: 5, 649 — 670
To link to this Article: DOI: 10.1080/00218464.2010.484318
URL: http://dx.doi.org/10.1080/00218464.2010.484318

The Journal of Adhesion, 86:649–670, 2010

ISSN: 0021-8464 print/1545-5823 online
DOI: 10.1080/00218464.2010.484318

Taylor & Francis
Taylor & Francis Group

Adhesively Bonded Repair Proposal for Wood Members Damaged by Horizontal Shear Using Carbon-Epoxy Patches

R. D. S. G. Campilho[1], M. F. S. F. de Moura[1], D. A. Ramantani[1], J. J. L. Morais[2], A. M. J. P. Barreto[1], and J. J. M. S. Domingues[3]

[1]Departamento de Engenharia Mecânica, Faculdade de Engenharia da Universidade do Porto, Porto, Portugal
[2]CITAB/UTAD, Departamento de Engenharias, Vila Real, Portugal
[3]Departamento de Engenharia Mecânica, Instituto Superior de Engenharia do Porto, Porto, Portugal

In this work, a repair technique with adhesively bonded carbon-epoxy patches is proposed for wood members damaged by horizontal shear and under bending loads. This damage is characterized by horizontal crack growth near the neutral plane of the wood beam, normally originating from checks and shakes. The repair consists of adhesively bonded carbon-epoxy patches on the vertical side faces of the beam at the cracked region to block sliding between the beam arms. An experimental and numerical parametric analysis was performed on the patch length. The numerical analysis used the finite element method (FEM) and cohesive zone models (CZMs), with an inverse modelling technique for the characterization of the adhesive layer. Trapezoidal cohesive laws in each pure mode were used to account for the ductility of the adhesive used. To fully reproduce the tests, horizontal damage propagation within the wood beam was also simulated. A good correlation with the experiments was found. Regarding the effectiveness of the repair, for the conditions selected for this work, a full strength recovery was achieved for the bigger value of patch length tested.

Keywords: Cohesive zone models; Composite; Finite element analysis; Repair; Wood

Received 22 June 2009; in final form 15 February 2010.

Presented in part at the 3rd International Conference on Advanced Computational Engineering and Experimenting (ACE-X 2009), Rome, Italy, 22–23 June 2009.

Address correspondence to R. D. S. G. Campilho, Department of Engineering Mechanics, Faculty of Engineering, University of Porto, Rua Dr. Roberto Frias s/n, Porto 4200-465, Portugal. E-mail: raulcampilho@hotmail.com

1. INTRODUCTION

Different scenarios can trigger the requirement of a repair intervention in large-scale wood members, such as natural defects, deterioration, and in-service damage. Natural defects in wood, like knots, splits, checks, wanes, or shakes, reduce its strength and durability [1–9], usually resulting from uneven drying and size variations [1,10]. These flaws are more detrimental to the tensile strength than to the compressive strength, since under tension they tend to develop into cracks. At these regions, the benefits of eventual superficial treatments applied to the wood members are also neutralized. Deterioration or decay is mainly caused by bacteria, moisture, fungi, and insects, degrading the hardness, stiffness, and strength of wood members, due to the breakage of their internal structure [11–13]. Deterioration can be stopped by treating the exposed surfaces of the wood with fungicides and pesticides [14]. In-service damage of wood can occur in different ways, *e.g.*, fatigue, overloads, earthquakes, human intervention, or adverse environmental conditions. The repair of damaged wood members is a viable alternative to their replacement, for cost saving purposes, and also owing to the increasing scarceness of large wood trunks. Recently, composite materials such as carbon-fibre reinforced plastics (CFRP) and glass-fibre reinforced plastics (GFRP) are being tested for structural strengthening and repair of wood members, due to their attractive characteristics [15–22]. These comprise a higher strength and lighter weight than conventional materials, easy manufacturing by pultrusion with continuously decreasing costs, immunity to corrosion and flexibility, amongst others. The pioneering studies concerning the use of composite plates to strengthen wood structures were related to the development of reinforcement strategies, mainly using the adhesive-bonding technique. Actually, adhesive-bonding of strengthening elements has already proved to be structurally efficient and economically competitive with mechanical fastening methods [23,24]. Theakston [25] addressed the reinforcement of wood members with resin-impregnated GFRP plates bonded with an epoxy adhesive. Experimental tests showed a 39% increase of the bending strength. Spaun [26] chose *E*-glass fibre rovings to reinforce wood beams, because of their reduced cost, and a phenol-resorcinol adhesive to bond the reinforcement. A significant increase of the unreinforced tensile strength was attained, in proportion to the fibre-volume fraction of the *E*-glass reinforcement. Leichti *et al*. [27]. reported on the installation of aramid-fibre reinforced glulam members for a pedestrian bridge in Oregon. Tingley [28] described a method of reinforcing glulam timber using aramid-fibre and GFRP laminates. Some works were also found on analytical models for reinforcement

schemes. In the paper of Chen and Balaguru [29], a non-linear analytical model was formulated for the analysis of reinforced wood members with composites. The comparative evaluation between the analytical and experimental data showed that the model provides accurate predictions. An analytical model was also developed by Plevris and Triantafillou [30] to predict the creep behaviour under bending of reinforced wood members with CFRP laminates bonded to the tension faces. The results were in good agreement with the analytical model. Research on the repair of wood members is still poor at the present time [9,12,31]. In the few available works, CFRP laminates or fabrics have been externally bonded using epoxy to strengthen the damaged zones. For beams under bending, unidirectional laminates are usually recommended in the tension or compressive faces, with the fibres aligned along the beam's length for maximum effectiveness [32–34]. Plate fastening techniques [9] or insertion of spikes running the beams height [12] are the most common methodologies to repair beams damaged by horizontal shear and to overcome the loss of shear properties of the beams. However, these studies are typically experimental; only a few of these have reported on comparisons with analytical predictions [33,34]. Concerning some experimental studies, Alam *et al*. [31] compared different repair strategies for wood beams damaged in the laboratory, to simulate structural damage, under four-point bending (4PB). The repair was executed by routing of grooves in the tension, compression, or both faces of the beams along their length, and adhesive-bonding of reinforcement rods with an epoxy adhesive. Steel and composite pultruded rods of CFRP, GFRP, and FULCRUM (commercial designation of a glass fibre reinforced polyurethane composite) with a rectangular section were tested. The results were compared with the undamaged beam strength. Regardless of the repair material, the stiffness and strength increased from repairing in the compression face to the repair on both faces. The steel and CFRP rods led to higher strengths than the undamaged beam, whilst the other materials were merely sufficient to restore the undamaged beam strength. Duarte *et al*. [35]. proposed a rehabilitation technique for wood members under bending that can be also feasible for repairing. The method consists of the removal of the decayed portions, followed by replacement with a reinforced portion of wood, bonded to the damaged structure with a reinforced epoxy mortar. Different reinforcements were tested, such as mild steel ribbed bars, stainless steel threaded rods, and pultruded GFRP bars. The experimental programme initiated with the test of undamaged beams up to failure. After a tension failure, the beams were recovered and tested again. The ultimate bending moment and the local and global moduli of elasticity were the collected data. The threaded rods were particularly effective, since

the thread enhanced friction with the epoxy mortar. The GFRP bars, although showing high tensile strength, have a smaller modulus of elasticity, resulting in larger deformations that are not accommodated by the surrounding mortar. As a consequence, severe cracking at the interface region led to a premature collapse.

In this work, an adhesively-bonded repair technique is proposed using carbon-epoxy patches for wood members of the *Pinus Pinaster* species damaged by horizontal shear and under bending loads. This damage is characterized by horizontal cracking near the neutral plane of the wood beam, normally originating from checks and shakes [1,13]. Wood members showing sharp changes in growth ring density or extremely low humidity contents are particularly likely to fail by horizontal shear [36]. Beyond the loss of strength, this fracture also causes a reduction of flexural stiffness. Actually, since the aspect ratio (height to length) of wood beams is relatively low, their flexural stiffness is strongly related to the shear performance [12]. The repair consists of adhesively bonded carbon-epoxy patches on the vertical side faces of the beam at the cracked region to block sliding between the beam arms. An experimental and numerical parametric analysis was performed on the patch length (L_P). The numerical analysis used the FEM and CZMs with trapezoidal laws for the adhesive layer fracture. To account for the experimental failures, horizontal fracture within the wood was also considered.

2. NUMERICAL ANALYSIS

2.1. Cohesive Zone Model

The cohesive fracture of a layer of the ductile epoxy adhesive 2015 by Araldite® (Huntsman, Basel, Switzerland) with $t_A = 0.2$ mm and horizontal damage propagation in the wood were simulated with a mixed-Mode (I+II+III) CZM. A trapezoidal law between stresses (σ) and relative displacements (δ_r) between homologous points of the cohesive elements with zero thickness was considered (Fig. 1), to account for the adhesive ductility [37–39], some modifications being introduced to simulate the brittle fracture of wood. The formulation allows a mixed-mode behaviour, in which damage onset is predicted using the quadratic stress criterion

$$\begin{aligned} &\left(\frac{\sigma_I}{\sigma_{u,I}}\right)^2+\left(\frac{\sigma_{II}}{\sigma_{u,II}}\right)^2+\left(\frac{\sigma_{III}}{\sigma_{u,III}}\right)^2=1 \quad \text{if} \quad \sigma_1>0 \\ &\left(\frac{\sigma_{II}}{\sigma_{u,II}}\right)^2+\left(\frac{\sigma_{III}}{\sigma_{u,III}}\right)^2=1 \qquad\qquad \text{if} \quad \sigma_1\leq 0, \end{aligned} \tag{1}$$

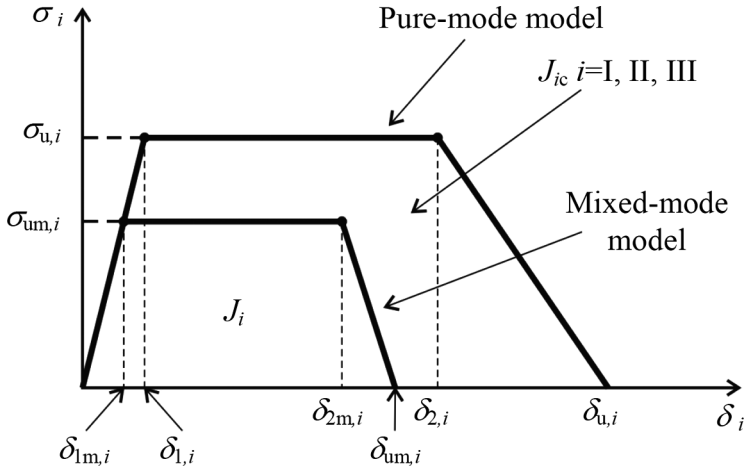

FIGURE 1 The trapezoidal softening law for pure-mode and mixed-mode.

where σ_i (i = I, II, III) represent the stresses in each mode and $\sigma_{u,i}$ (i = I, II, III) the corresponding local strengths. Equation (1) can be rewritten as a function of the relative displacements

$$\left(\frac{\delta_{1m,I}}{\delta_{1,I}}\right)^2+\left(\frac{\delta_{1m,II}}{\delta_{1,II}}\right)^2+\left(\frac{\delta_{1m,III}}{\delta_{1,III}}\right)^2=1. \tag{3}$$

$\delta_{1,i}$ (i = I, II, III) are the pure-mode relative displacements at damage initiation and $\delta_{1m,i}$ (i = I, II, III) the corresponding mixed-mode ones. Stress softening onset was predicted using a criterion similar to (2)

$$\left(\frac{\delta_{2m,I}}{\delta_{2,I}}\right)^2+\left(\frac{\delta_{2m,II}}{\delta_{2,II}}\right)^2+\left(\frac{\delta_{2m,III}}{\delta_{2,III}}\right)^2=1. \tag{3}$$

$\delta_{2,i}$ (i = I, II, III) are the relative displacements in pure-mode at stress softening onset and $\delta_{2m,i}$ (i = I, II, III) the corresponding mixed-mode ones. Crack growth was simulated by the linear energetic criterion

$$\frac{J_I}{J_{Ic}}+\frac{J_{II}}{J_{IIc}}+\frac{J_{III}}{J_{IIIc}}=1, \tag{4}$$

being J_{ic} (i = I, II, III), the fracture energy in the respective pure-mode. When Eq. (4) is satisfied at a given integration point, damage grows and stresses are released, apart from normal compressive ones. A detailed description of this model can be found in the work of Campilho *et al*. [40].

2.2. Cohesive Laws Definition

Considerable research has been conducted in the past to determine the correct cohesive laws for adhesive layers under different adhesive/adherend systems [41,42]. In fact, although the precise description of the law is always important from a fundamental perspective [43], often an approximated parameterized shape is established for the numerical prediction of damage growth. To model the response of a $t_A = 0.2$ mm layer of Araldite® 2015, which is known to endure extensive plastic deformation at an approximately constant load, the trapezoidal relationship of Fig. 1 was established. The formulation is, thus, simplified by the use of linear segments for the elastic, plastic, and decaying portions of the law [44]. In these laws, $\sigma_{u,i}$ and J_{ic} ($i = $ I, II, III) are considered to be the most important parameters for the output of the simulations [43,45]. On the determination of these parameters, a consensus exists about the testing methods to be employed. However, some issues concerning the use of these tests still subsist, due to the existence of constraint effects that affect these variables. In fact, the adherends' deformation and deflection affect the stress and strain distributions and, accordingly, the damaged region within the adhesive layer [46,47]. Apart from this, the width and value of t_A of the adhesive layer also have an impact on the stress and strain distributions in the adhesive. For instance, a change of t_A can be the origin of a transition from small-scale yielding conditions within the adhesive to fully plastic conditions [48]. Because of the these issues, the cohesive parameters of adhesive layers substantially vary with the value of t_A [49]. To account for these variations, in this work, the cohesive laws of the adhesive layer in pure-Modes I and II were estimated by double cantilever beam (DCB) (Mode I) and end-notched flexure (ENF) (Mode II) tests with the same value of t_A, using inverse modelling [50–52]. The pure Mode III cohesive law was equated to the pure Mode II one, as an approximation. These methods constitute the most viable option to solve the multi-parameter dependency of physical experiments in numerical models [43]. The adhesive layer elastic stiffness in tension and shear (up to $\delta_{1,i}$, Fig. 1) was specified from the experimentally measured values of Young's modulus ($E = 1850$ MPa) and shear modulus ($G = 650$ MPa) [53], as detailed in the work of Campilho *et al.* [40]. Failure within the wood (Fig. 2) in the *RL* plane (horizontal longitudinal plane of the beam) is also accounted for to reproduce the experiments, the cohesive parameters of which were established from previous works [54]. Owing to the brittle behaviour of wood in shear, the cohesive laws in each pure-mode for an *RL* fracture of wood were converted to triangular shapes ($\delta_{2,i} = \delta_{1,i}$ in Fig. 1), and a penalty

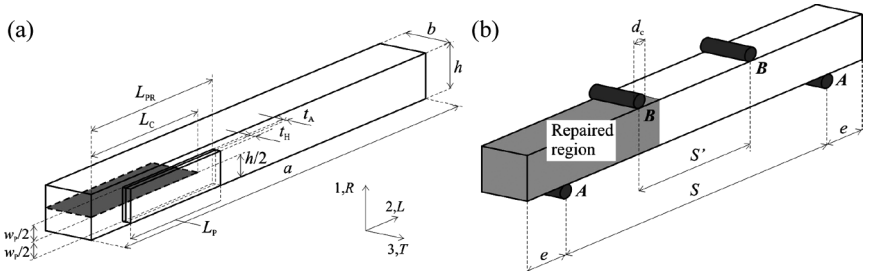

FIGURE 2 Schematic representation of the repair with (a) the characteristic dimensions and (b) test setup.

function method was used up to $\sigma_{u,i}$ (Fig. 1). Table 1 summarizes the cohesive parameters for the adhesive and wood fractures [38,54].

2.3. Numerical Models

Fig. 2 shows the repair geometry and testing conditions. The horizontal shear crack was equated at the middle of the beam height (Fig. 2a) [9]. Repairing consists of bonding of CFRP patches on the vertical side faces of the beam at the cracked region to block sliding between the beam arms. The patches consist on unidirectional laminates with the fibres aligned vertically, to maximize their shear strength in the horizontal *RL* plane. Figure 2a shows the beam length (a), width (b) and height (h), crack length (L_C), adhesive thickness (t_A), patch thickness (t_H), distance between the beam and patch edges (L_{PR}), patch width (w_P), and L_P (Table 2). The value of L_{PR} was always kept constant, while varying L_P (45, 75, and 105 mm). Figure 3 shows the mesh of (a) the $L_P = 45$ mm repair and (b) respective details at the patch and (c) crack tip regions. The FEM simulations were performed in ABAQUS®, including geometrical non-linearities, using eight-node hexahedral solid elements. Vertical symmetry conditions were considered to model only half-width of the beam. The wood and CFRP

TABLE 1 Cohesive Parameters in Pure-Modes I and II Used to Simulate Different Failures

Cohesive laws	i	J_{ic} [N/mm]	$\sigma_{u,i}$ [MPa]	$\delta_{2,i}$ [mm]	$\delta_{u,i}$ [mm]
Adhesive layer	I	0.43	23.0	0.0187	0.021
	II	4.70	22.8	0.1710	0.248
Wood in the *RL* plane	I	0.2	16	$1.6 * 10^{-5}$	0.025
	II	1.2	16	$1.6 * 10^{-5}$	0.150

TABLE 2 Dimensions and Testing Parameters (in mm) of the Repairs

Dimensions				
$a = 300$	$b = 20$	$h = 20$	$L_C = 95$	$t_A = 0.2$
$t_H = 1.2$	$L_{PR} = 105$	$w_P = 4.5$	$L_P = 45$, 75 and 105	
Testing parameters				
$S = 260$	$S' = 130$	$d_C = 10$	$e = 20$	

patches were modelled as elastic orthotropic materials, with the properties of wood given in Table 3 [54] and of the laminas of CFRP shown in Table 4 [55]. The beam regions contacting the cylinders were refined with 40 elements along a length of 2.5 mm. In addition, the mesh was set to present a higher refinement near the crack tip, to assure stable crack initiation and growth. The repaired region of the beam was also more refined than the undamaged portion. Four elements were employed to model the beams' half-width, and eight elements to model their height. In both cases, different element sizes were selected, using bigger elements where approximately constant stresses are expected. The patch thickness was modelled with two

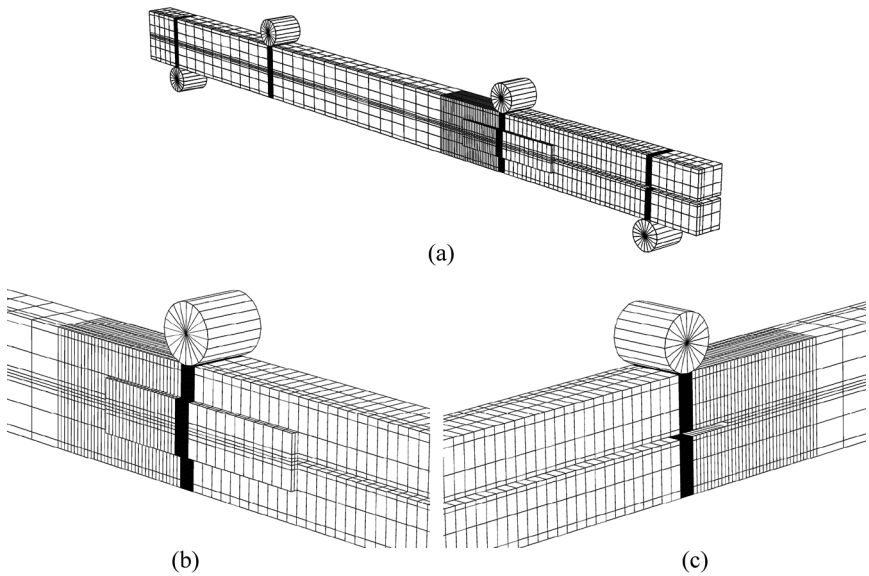

FIGURE 3 Mesh for (a) the $L_P = 45$ mm repair and (b) details at the patch and (c) crack tip regions.

TABLE 3 Elastic Orthotropic Properties of Wood Species *Pinus Pinaster*

$E_L = 10.2\,\text{GPa}$	$\nu_{LR} = 0.342$	$G_{LR} = 1120\,\text{MPa}$
$E_R = 1010\,\text{MPa}$	$\nu_{LT} = 0.342$	$G_{LT} = 1040\,\text{MPa}$
$E_T = 1010\,\text{MPa}$	$\nu_{RT} = 0.380$	$G_{RT} = 170\,\text{MPa}$

TABLE 4 Elastic Orthotropic Properties of a Unidirectional Lamina of CFRP

$E_1 = 109\,\text{GPa}$	$\nu_{12} = 0.342$	$G_{12} = 4315\,\text{MPa}$
$E_2 = 8819\,\text{MPa}$	$\nu_{13} = 0.342$	$G_{13} = 4315\,\text{MPa}$
$E_3 = 8819\,\text{MPa}$	$\nu_{23} = 0.380$	$G_{23} = 3200\,\text{MPa}$

elements. For consistency with the fabricated specimens, a 1-mm gap was left between the cracked beam arms (Fig. 3). A blunt region resulted from the mesh construction at the tip of the horizontal shear crack. This corresponds approximately to the obtained shape after cutting the crack with a 1-mm thickness saw. To accurately reproduce the specimens tested, the two nodes of the cohesive elements corresponding to the two solid elements nearest to the crack tip were separated from the beginning of the analysis, imposing in the numerical models that $\delta > \delta_{u,i}$ (Fig. 1), which, in turn, completely released normal and shear stresses between these nodes. As a result, the original crack was extended by 1 mm. In the fabricated specimens, a sharp crack tip was induced with a razor blade. The value of L_C, extending up to the crack tip, corresponds in the FEM models to the initiation of the third cohesive element. Concerning the cohesive elements loci to simulate damage growth, these were used for the adhesive layer and *RL* propagation initiating at the tip of the horizontal shear crack. It should be mentioned that other fracture mechanisms were found in the experiments, such as tensile failure below the loading cylinders or cross-grain tension failure (at a small angle to the beam's L direction, due to minor fibre misalignment). However, since these fractures always occurred after the maximum load of the repairs (P_m), they were not considered as relevant.

3. EXPERIMENTAL WORK

The experimental programme involves three different repair geometries and also the unrepaired (cracked) beam. Results for the undamaged beam were obtained from a previous work [56]. A smaller

value of w_P was selected compared with h to avoid interferences between the patches and the cylinders. The patches were fabricated using CFRP prepreg (Texipreg HS 160 RM from SEAL®, Legnano, Italy) with 0.15 mm of ply thickness. The value of t_H was tuned numerically as the minimum value assuring that the typical shear strengths of the CFRP patch in the *RL* plane were not attained up to the repair fracture, to avoid premature patch failures [57]. Figure 2 (b) shows the testing configuration under 4PB (Table 2). ***A*** and ***B*** represent the supporting and loading cylinders, respectively. The axes 1, 2, 3 of Fig. 2 correspond to the fibre, transverse, and thickness directions of the unidirectional patch, respectively. The *R, L, T* coordinate system pertains to the wood orientations (fibres' longitudinal direction (*L*), rings' radial direction (*R*), and rings' tangential direction (*T*)). In adhesively bonded repairs of full-scale elements, the preparation of the bonding surfaces is particularly meaningful. Actually, bonding is made difficult by the use of preservatives on the wood, which degrade the bonding performance, by eventual splits or other flaws, and by irregular surfaces [12]. These issues must be accounted for in the repair's fabrication, and proper surface activation of the wood must be guaranteed for a strong bond [58–60]. In the fabricated specimens these problems are less significant, since they are cut to their final dimensions with an automated technique that yields flat bonding surfaces, and since specimens with defects are also discarded. Nevertheless, for optimal results, the wood bonding surfaces were abraded and cleaned with compressed air [61]. The same approach was followed for the CFRP patches bonding regions, acetone being used for cleaning. Application of the adhesive (Araldite® 2015) was performed manually in thin strips with the manufacturer's dispensing gun and mixing nozzle. Since the correctness of t_A has a significant effect on the adhesive mechanical properties, special attention was paid to guarantee the value of 0.2 mm. To this end, nylon fishing lines were used as stoppers near the patch edges. After curing at room temperature, the specimens were tested in an Instron® (Norwood, MA, USA) 1125 testing machine with a 100kN load cell, at room temperature, and under displacement control (2 mm/min). From the ten specimens tested for each condition, at least seven valid results were always obtained.

4. RESULTS

4.1. Numerical

A detailed analysis of the most significant stresses in the adhesive layer is presented, allowing an easier interpretation of the

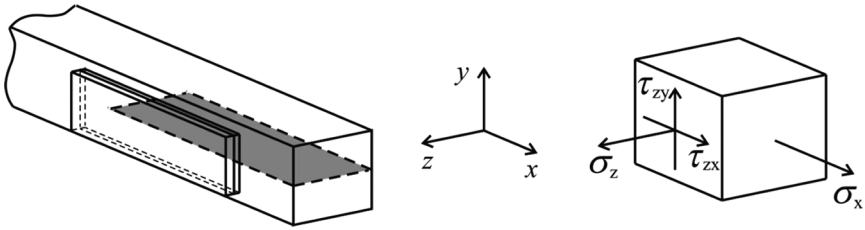

FIGURE 4 Stress components evaluated for the horizontal shear failure repairs.

experimental and numerical failure mechanisms and strength tendencies. Figure 4 shows the coordinate system used and the most relevant stress components for these repairs, based on a detailed analysis of the six stress components distributions in the repair, particularly in the adhesive layer. σ_z, τ_{zx}, and τ_{zy} stresses will be evaluated. σ_x stresses for the $L_P = 45$ mm repair under a displacement of the loading cylinders (δ) of 15 mm are initially presented (Fig. 5). The two beam arms at the cracked edge initiate contact and relative sliding before the patch detachment. σ_x stresses outside the repair region follow the expected behaviour of members under bending, varying linearly in the h-direction with the distance to the neutral axis (compressive stresses at the upper half and tensile ones at the lower half). In the patch, σ_x stresses are approximately nil, except at its edge nearest to

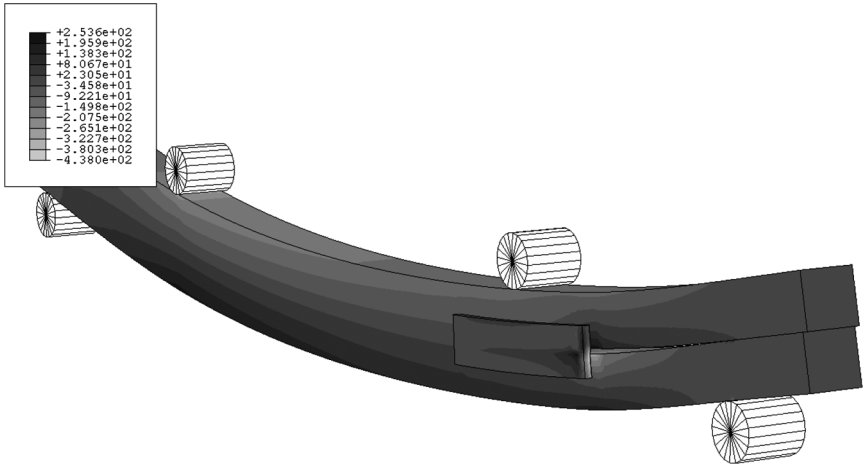

FIGURE 5 σ_x stresses [MPa] in the repaired beam ($L_P = 45$ mm repair).

the cracked end of the beam (from this point addressed as *loaded edge*). The following figures illustrate the most significant stress components in the adhesive layer for the $L_P = 45$ and 105 mm repairs, considering the repair orientation of Fig. 5, and for a value of δ of 0.3 mm and magnification of 50×. These include σ_z (Fig. 6), τ_{zx} (Fig. 7), and τ_{zy} (Fig. 8) stresses. It should be emphasized that σ_z, τ_{zx}, and τ_{zy} stresses are approximately constant in the adhesive thickness direction in all the figures in this study, showing only minor variations near the loaded edge of the patch. σ_z stresses or the $L_P = 45$ and 75 mm repairs are nearly nil except at the loaded edge, anticipating

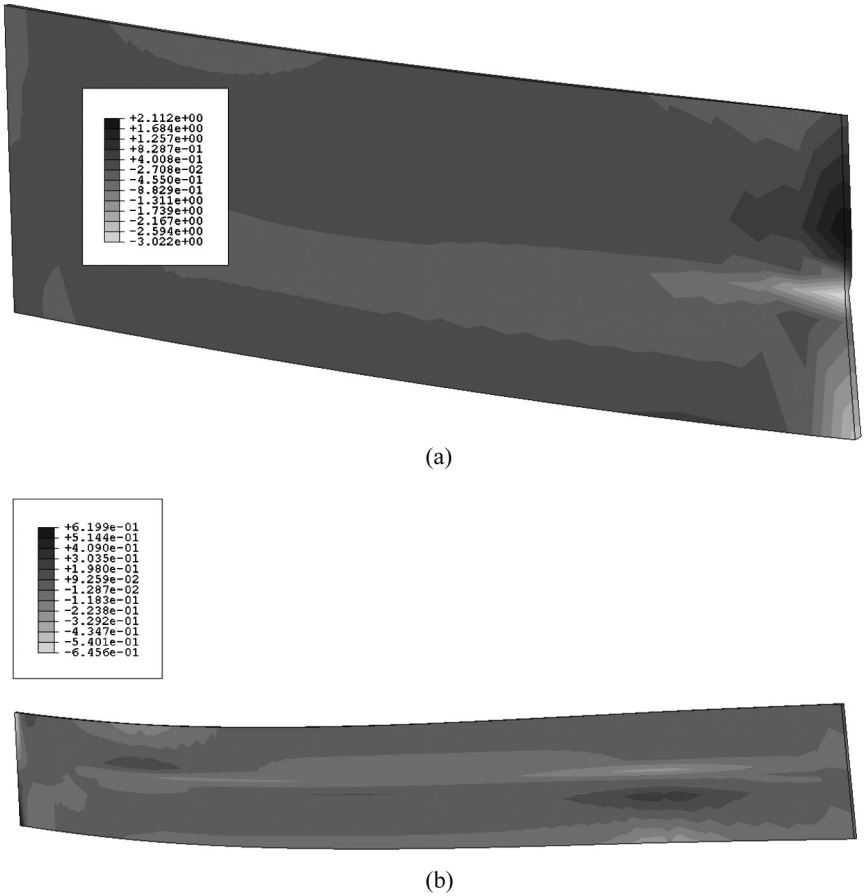

FIGURE 6 σ_z stresses [MPa] at the repair region for the (a) $L_P = 45$ mm and (b) $L_P = 105$ mm repairs.

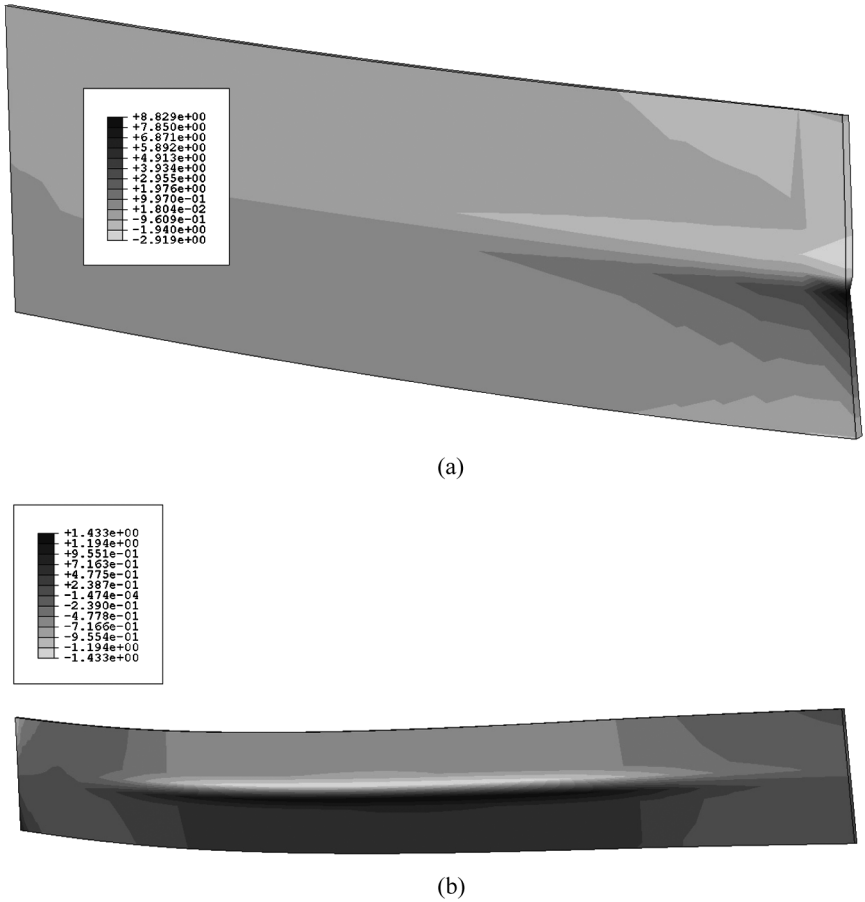

FIGURE 7 τ_{zx} stresses [MPa] at the repair region for the (a) $L_P = 45$ mm and (b) $L_P = 105$ mm repairs.

eventual peel failure at this region. For the $L_P = 105$ mm repair, the patch extends up to the beam edge, which resulted in a different behaviour, with σ_z stress concentrations near the crack gap above the supporting cylinder. τ_{zx} stresses in the adhesive layer emerge due to the shearing tendency between the beam arms, being negligible in most of the adhesive layer, except at the loaded edge ($L_P = 45$ and 75 mm repairs). Conversely, for the $L_P = 105$ mm repair, τ_{zx} stresses peak at both sides of the crack gap, extending from the tip of the horizontal shear crack to the supporting cylinder. τ_{zy} stresses, on the other hand, appear due to the existence of the 1-mm gap between

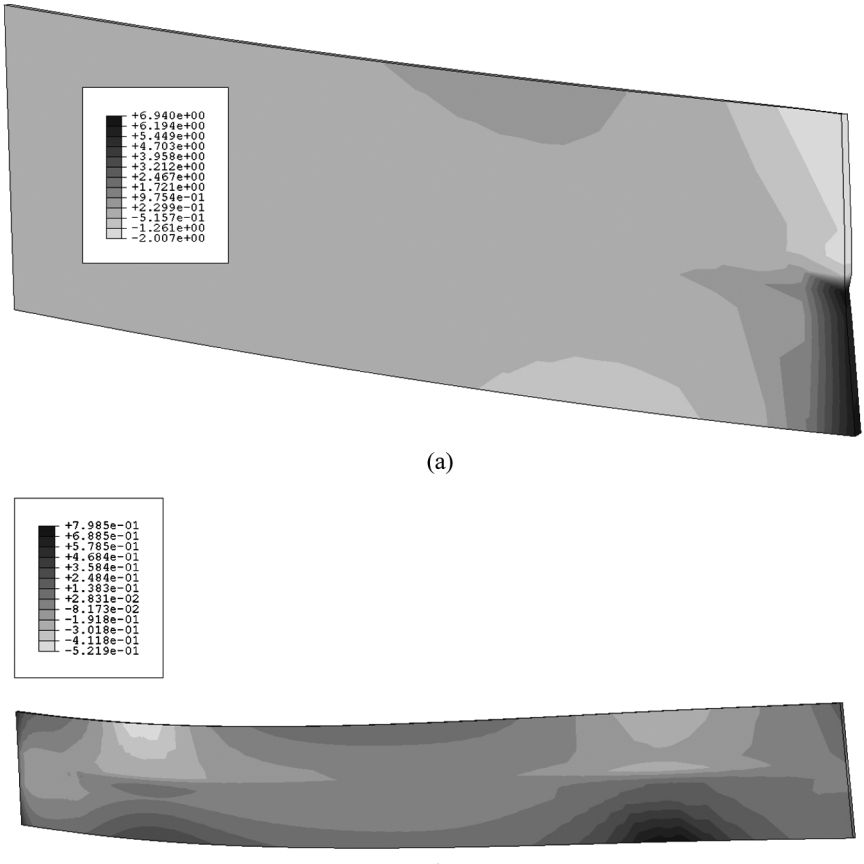

FIGURE 8 τ_{zy} stresses [MPa] at the repair region for the (a) $L_P = 45$ mm and (b) $L_P = 105$ mm repairs.

the wood beam arms, which tends to close due to the loading applied, causing vertical shear. Oppositely to τ_{zx} stresses, τ_{zy} ones are more concentrated towards the loaded edge of the adhesive ($L_P = 45$ and 75 mm repairs). Following the previous results, for the $L_P = 105$ mm repair, τ_{zy} peak stresses at the loaded edge disappear, giving rise to moderate τ_{zy} stresses above the supporting cylinder. The magnitude of σ_z, τ_{zx}, and τ_{zy} peak stresses diminishes from the $L_P = 45$ mm to the $L_P = 105$ mm repair. In these repairs, damage is expected to initiate by an adhesive layer failure (or in the wood beam near the adhesive layer) due to sliding between the beam arms, prior to damage

propagation at the tip of the horizontal shear crack. The stress analysis conducted shows that P_m (hypothetically corresponding to damage initiation in the adhesive layer or near in the wood beam) is likely to increase with L_P, since all three stress components evaluated diminish progressively with this parameter. Additionally, bigger values of L_P increase the shear resistant area of the patches. The locus of peak stresses is the same between all stress components (at the loaded edge), suggesting that damage initiates at this region.

The FEM fractures are equally characterized. The undamaged beam results showed a pure tension fracture below the loading cylinders [56]. For the unrepaired beam, P_m was achieved due to an extensive *RL* propagation of the horizontal shear crack (Fig. 9a). The $L_P = 45$ mm and $L_P = 75$ mm repairs behaved similarly, with evidence of damage prior to P_m by patch debonding at the loaded edge (Fig. 9b; $L_P = 75$ mm repair) due to the aforementioned stress concentrations (Figs. 6–8). After this, the load (P) continued to increase up to P_m. Failure occurred due to a complete debonding between the patch

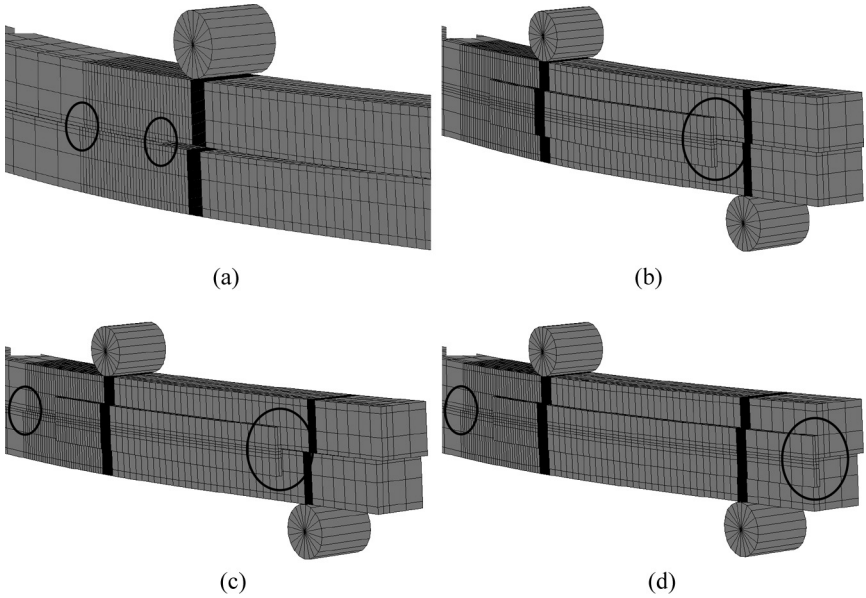

FIGURE 9 Numerical failures: (a) at the horizontal shear crack tip for the unrepaired beam, (b) initiating at the adhesive layer loaded edge, (c) growing within the adhesive layer and by *RL* crack propagation for the $L_P = 75$ mm repair, and (d) after complete failure for the $L_P = 105$ mm repair. The circle marks highlight the regions of damage.

and the lower beam arm, simultaneously with *RL* crack propagation starting at the tip of the horizontal shear crack (Fig. 9c; $L_P = 75$ mm repair). This event can be confirmed by the sliding of the solid finite elements simulating the wood beam at the transition between the differently refined meshes (marked with a circle). This also applies to the subsequent repair. The last repair ($L_P = 105$ mm) showed numerically an abrupt cohesive failure of the adhesive layer between the patch and the lower beam arm, growing rapidly to all of the extent of the patch. This caused a drop of P_m, with final failure by *RL* propagation initiating at the horizontal shear crack (Fig. 9d).

4.2. Experimental

The experimental fracture mechanisms, which were equivalent to the FEM results, are described. The undamaged wood beam attained experimentally P_m by a pure tension fracture below the loading cylinders [56]. For the unrepaired beam, P_m is associated with extensive crack growth, initiating at the horizontal shear crack tip (Fig. 10a), which is more easily identified by the sliding of the vertical lines at the crack tip, since crack propagation in wood under shear is not clearly visible [62,63]. The $L_P = 45$ mm and $L_P = 75$ mm repairs fractured identically, with a premature patch detachment prior to P_m at the loaded edge (Fig. 10b; $L_P = 75$ mm repairs). The locus of damage initiation is related to the regions of σ_z, τ_{zx}, and τ_{zy} stress

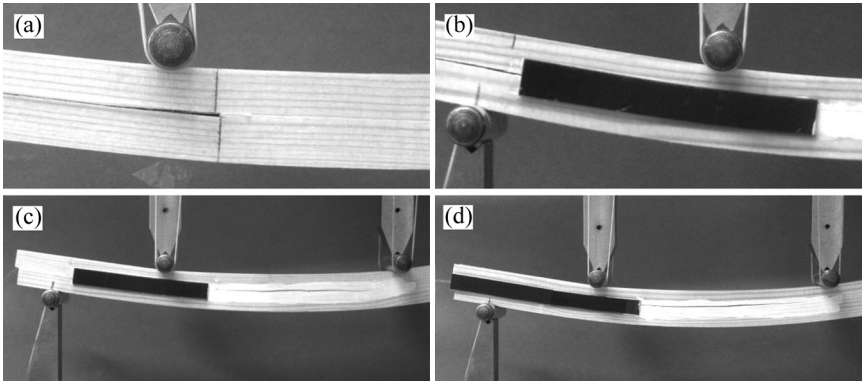

FIGURE 10 Experimental failures: (a) at the horizontal shear crack tip for the unrepaired beam, (b) initiating at the adhesive layer loaded edge, (c) growing within the adhesive layer and by *RL* crack propagation for the $L_P = 75$ mm repair, and (d) after complete failure for the $L_P = 105$ mm repair.

concentrations (respectively, Figs. 6–8). Following, P continued to grow as δ increased, with crack propagation towards the horizontal shear crack tip. After extensive patch damage, P_m was achieved similarly to the unrepaired beam, *i.e.,* by crack propagation starting from the horizontal shear crack tip (Fig. 10c; $L_P = 75$ mm repairs). Damage was always simultaneous at the two patches. For the $L_P = 105$ mm repairs, P_m was related to patch detachment at the upper or lower beam arm, by a cohesive failure of the adhesive layer. This failure occurred abruptly from the repair edge up to near the loading cylinder. This is consistent with the stress analysis performed, showing an identical magnitude of τ_{zx} stresses, which are the most significant stress components in the repair, between these two regions (Fig. 7b). Figure 10d shows a posterior stage of damage, after extensive *RL* crack propagation.

4.3. Experimental/Numerical Comparison

The unrepaired beam load-displacement (P-δ) curves (Fig. 11) are shown to be in close agreement. For both the experiments and the simulations, P_m corresponded to extensive damage growth at the tip of the horizontal shear crack. The FEM curve of the $L_P = 75$ mm repairs (Fig. 12) clearly reflects the premature damage at the loaded

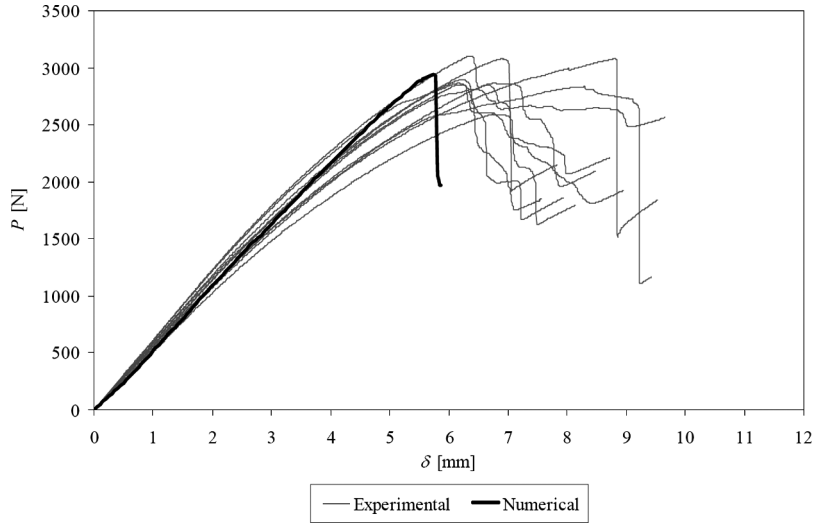

FIGURE 11 Experimental and numerical P-δ curves for the unrepaired beam.

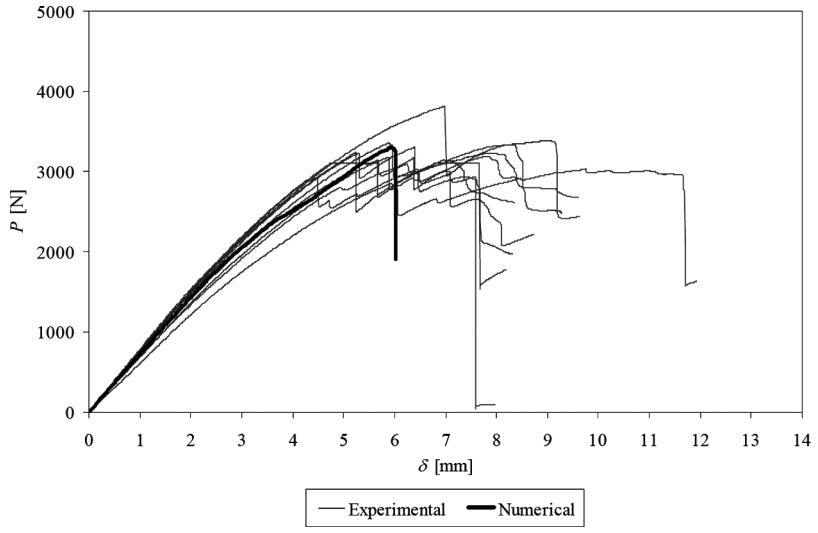

FIGURE 12 Experimental and numerical P-δ curves for the $L_P = 75$ mm repair.

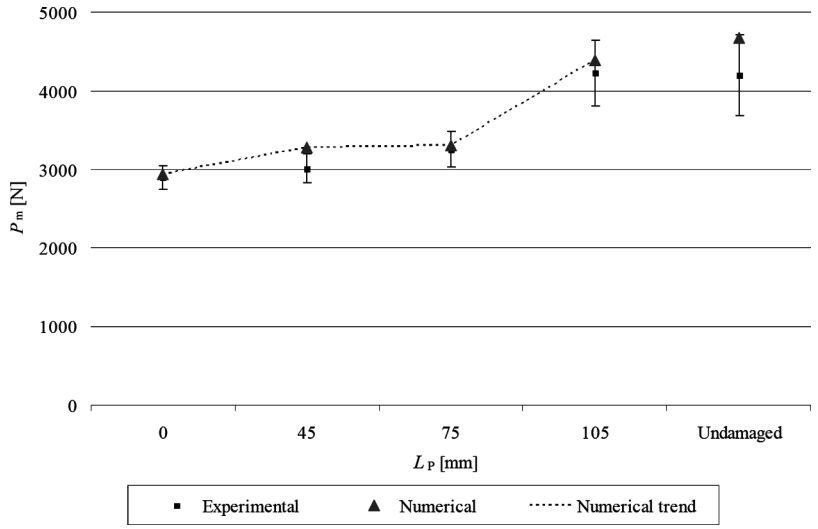

FIGURE 13 P_m as a function of L_P. Experimental results, numerical predictions, and respective tendency as a function of L_P.

edge (at $\delta \approx 4\,\text{mm}$), which was related to a cohesive failure of the adhesive layer. The predictions of P_m and the corresponding experimental average values and deviations are compared in Fig. 13. The accurate predictions confirm the suitability of the FEM methodology followed in this work. These results show an approximate 30% reduction of P_m inducing the horizontal shear crack in the specimens, and also that the $L_P = 45$ and 75 mm repairs practically do not affect the value of P_m. This is related to the cohesive failure of the adhesive layer and *RL* crack propagation occurring prematurely or near the P_m value for the unrepaired beam. Oppositely, the $L_P = 105\,\text{mm}$ repair led to a significant improvement in P_m, which approached the strength of the undamaged beam. Actually, under this configuration the patch prevented the sliding of the beam arms and consequent failure by *RL* propagation up to near the value of P_m of the undamaged beam. The experimental scatter of these results is justified mainly by variations in wood properties [64,65].

5. CONCLUDING REMARKS

In this work, an adhesively bonded repair technique using adhesively bonded carbon-epoxy patches was tested for wood members of the *Pinus Pinaster* species damaged by horizontal shear and under bending loads. This damage is characterized by horizontal crack growth near the neutral plane of the wood beam. The repair consisted of adhesively bonded carbon-epoxy patches on the vertical side faces of the beam at the cracked region. An experimental and numerical parametric analysis was performed on the patch length. The numerical analysis used the finite element method and cohesive zone modelling, including inverse modelling for the characterization of the adhesive as a thin layer. Trapezoidal cohesive laws in pure-Modes I and II were used to account for its ductility. Horizontal damage propagation within the wood was also simulated. The accurate predictions validate the numerical methodology, which will reduce the time and cost associated with extensive experimentation. For the particular materials and dimensions employed, the repair with patch length of 105 mm practically restores the undamaged strength of the beam. Values up to 75 mm were ineffective, due to patch detachment for loads smaller than or of the same order of magnitude as, the unrepaired beam strength.

ACKNOWLEDGMENTS

The authors would like to thank the Portuguese Foundation for Science and Technology for supporting the work presented here,

through the individual grant SFRH/BD/30305/2006 and the research project PDTC/EME-PME/64839/2006.

REFERENCES

[1] Bodig, J. and Jayne, B. A., *Mechanics of Wood and Wood Composites*, (Van Nostrand Reinhold Company, New York, 1982).
[2] Rammer, D. R. and McLean, D. I., Shear Strength of Wood Beams, Proc. National Conference on Wood Transportation Structures, (Madison, Wisconsin, USA, 23–25 October, 1996).
[3] Rammer, D. R., McLean, D. I., and Cofer, W. F., In-place Shear Strength of Wood Beams, Proc. 5th World Conference on Timber Engineering, (Montreux, Switzerland, 17–20 August, 1998).
[4] Rammer, D. R., Evaluation of recycled timber members. Materials and construction, Proc. 5th ASCE Materials Engineering Congress, (Cincinnati, USA, 10–12 May, 1999).
[5] Falk, R. H., Green, D., Rammer, D., and Lantz, S. F., *Forest Prod. J.* **60**, 71–76 (2000).
[6] Green, D. W., Falk, R. H., and Lantz, S. F., *Forest Prod. J.* **51**, 82–88 (2001).
[7] Lee, S. M., Abbott, A. L., and Schmoldt, D. L., *Comput. Electron. Agr.* **41**, 121–137 (2003).
[8] Christy, A. G., Senden, T. J., and Evans, P. D., *Measurement* **37**, 109–118 (2005).
[9] Akbiyik, A., Lamanna, A. J., and Hale, W. M., *Construct. Build. Mater.* **21**, 991–1000 (2007).
[10] Ou, F. L. and Weller, C., *Transport. Res. Rec.* **1053**, 1–12 (1986).
[11] Watt, D. and Swallow, P., *Surveying Historic Buildings*, (Donhead Publishing, Shaftesbury, 1996).
[12] Radford, D. W., Van Goethem, D., Gutkowski, R. M., and Peterson, M. L., *Construct. Build. Mater.* **16**, 417–425 (2002).
[13] Akbiyik, A., "Feasibility investigation into shear repair of timber bridge stringers," M.Sc. Thesis, Tulane University, New Orleans, (2005).
[14] Richardson, B., *Remedial Treatment of Buildings*, 2nd ed., (Butterworths/Heinemann, Stoneham, 1995).
[15] Sonti, S. S., Davalos, F. J., Zipfel, M. G., and GangaRao, H. V. S., *Forest Prod. J.* **45**, 55–58 (1995).
[16] Dorey, A. B. and Cheng, J. J. R., The Behavior of GFRP Glued Laminated Timber Beams. Advanced Composite Materials in Bridges and Structures, Proc. 2nd International Conference, (Montreal, Canada, August, 1996).
[17] Sonti, S. S. and GangaRao, H. V. S., Banding Timber Crossties Using Composite Fabrics for Improving Their Performance, Proc. 4th Materials Engineering Conference (Washington, DC, USA, November 10–14, 1996).
[18] Zaboklicki, A. and Gebski, M., Continuity of Wooden Beams as a Method of Reinforcement and Preservation of Timber Structures at Monumental Buildings, *Proc. International Conference on Structural Studies, Repairs and Maintenance of Historical Buildings Nr.5*, (San Sebastian, Spain, 25–27 June, 1997).
[19] Qiao, P., Davalos, J. F., and Zipfel, M. G., *Compos. Struct.* **41**, 87–96 (1998).
[20] Davalos, J. F., Zipfel, M. G., and Qiao, P., *J. Compos. Construct.* **3**, 92–100 (1999).
[21] Gentile, C., Svecova, D., and Rizkalla, S. H., *J. Compos. Construct.* **6**, 11–20 (2002).
[22] Chamarthy, R. and GangaRao, H., *SAMPE J.* **39**, 25–33 (2003).

[23] Dagher, H. J. and Lindyberg, R., FRP-wood hybrids for bridges: A comparison of E-glass and carbon reinforcements, *Proc. Structures Congress*, (Philadelphia, USA, 7–10 May, 2000).
[24] Custódio, J., Broughton, J., and Cruz, H., *Int. J. Adhes. Adhes.* **29**, 173–185 (2009).
[25] Theakston, F. H., *Canadian Agr. Eng.* ***January***, 17–19 (1965).
[26] Spaun, F. D., *Forest Prod. J.* **31**, 26–33 (1981).
[27] Leichti, R. J., Gilham, P. C., and Tingley, D. A., *Wood Design Focus* **4**, 3–4 (1993).
[28] Tingley, D. A., Aligned fiber reinforcement panel for structural wood members, US Patent 5362545.
[29] Chen, Y. and Balaguru, P. N., Fiber Reinforced Polymers (FRP) for Strengthening Timber Beams. *Proc. 47th International SAMPE Symposium and Exhibition*, (Long Beach, USA, 12–16 May, 2002).
[30] Plevris, N. and Triantafillou, T. C., *J. Struct. Eng.* **121**, 174–186 (1995).
[31] Alam, P., Ansell, M. P., and Smedley, D., *Compos. Part B – Eng.* **40**, 95–106 (2009).
[32] Bakis, C. E., Bank, L. C., Brown, V. L., Cosenza, E., Davalos, J. F., Lesko, J. J., Machida, A., Rizkalla, S. H., and Triantafillou, T. C., *J. Compos. Construct.* **6**, 73–87 (2002).
[33] Triantafillou, T. C., *J. Mater. Civil Eng.* **9**, 65–69 (1997).
[34] Triantafillou, T. C., *Compos. Sci. Technol.* **58**, 1285–1295 (1998).
[35] Duarte, A., Negrão, J., and Cruz, H., Rehabilitation of timber beams with reinforced epoxy plates, *Proc. 8th World Conference on Timber Engineering*, (Lahti, Finland, 14–17 June, 2004).
[36] Bodig, J. and Jayne, B. A., *Mechanics of Wood and Wood Composites*, (Krieger Publishing Company, Florida, 1993).
[37] Campilho, R. D. S. G., de Moura, M. F. S. F., and Domingues, J. J. M. S., *Int. J. Solids Struct.* **45**, 1497–1512 (2008).
[38] Campilho, R. D. S. G., de Moura, M. F. S. F., Pinto, A. M. G., Morais, J. J. L., and Domingues, J. J. M. S., *Compos. Part B – Eng.* **40**, 149–157 (2009).
[39] Campilho, R. D. S. G., de Moura, M. F. S. F., Ramantani, D. A., Morais, J. J. L., and Domingues, J. J. M. S., *J. Adhes. Sci. Technol.* **23**, 1493–1513 (2009).
[40] Campilho, R. D. S. G., de Moura, M. F. S. F., Ramantani, D. A., Morais, J. J. L., and Domingues, J. J. M. S., *Int. J. Adhes. Adhes.* **29**, 678–686 (2009).
[41] Sorensen, B. F. and Kirkegaard, P., *Eng. Fract. Mech.* **73**, 2642–2661 (2006).
[42] Leffler, K., Alfredsson, K., and Stigh, U., *Int. J. Solids Struct.* **44**, 530–545 (2007).
[43] Gustafson, P. A. and Waas, M., *Int. J. Solids Struct.* **46**, 2201–2215 (2009).
[44] Gustafson, P. A. and Waas, A. M., Efficient and robust traction laws for the modeling of adhesively bonded joints, Proc. AIAA/ASME/ASCE/ AHS/ASC 49th Structures, Structural Dynamics, and Materials Conference, (Schaumburg, USA, April 7–10, 2008).
[45] Bazant, Z. P., *Adv. Cement. Base. Mater.* **4**, 128–137 (1996).
[46] Wang, R. X., Sinclair, A. N., and Spelt, J. K., *J. Adhesion* **79**, 49–66 (2003).
[47] Pardoen, T., Ferracin, T., Landis, C. M., and Delannay, F., *J. Mech. Phys. Solid.* **53**, 1951–1983 (2005).
[48] Ikeda, T., Yamashita, A., Lee, D., and Miyazaki, N., *J. Eng. Mater. Tech.* **122**, 80–85 (2000).
[49] Xie, D. and Waas, A. M., *Eng. Fract. Mech.* **73**, 1783–1796 (2006).
[50] de Moura, M. F. S. F., Gonçalves, J. P. M., Chousal, J. A. G., and Campilho, R. D. S. G., *Int. J. Adhes. Adhes.* **28**, 419–426 (2008).
[51] de Moura, M. F. S. F., Campilho, R. D. S. G., and Gonçalves, J. P. M., *Compos. Sci. Technol.* **68**, 2224–2230 (2008).

[52] de Moura, M. F. S. F., Campilho, R. D. S. G., and Gonçalves, J. P. M., *Int. J. Solids Struct.* **46**, 1589–1595 (2009).
[53] Marques, E. A. S. and da Silva, L. F. M., *J. Adhesion* **84**, 917–936 (2008).
[54] Silva, M. A. L., de Moura, M. F. S. F., and Morais, J. J. L., *Compos. Part A – Appl. Sci.* **37**, 1334–1344 (2006).
[55] Campilho, R. D. S. G., de Moura, M. F. S. F., and Domingues, J. J. M. S., *Compos. Sci. Technol.* **65**, 1948–1958 (2005).
[56] Campilho, R. D. S. G., de Moura, M. F. S. F., Barreto, A. M. J. P., Morais, J. J. L., and Domingues, J. J. M. S., *Compos. Part A – Appl. Sci.* **40**, 852–859 (2009).
[57] Campilho, R. D. S. G., de Moura, M. F. S. F., Barreto, A. M. J. P., Morais, J. J. L., and Domingues, J. J. M. S., *Construct. Build. Mater*. doi: 10.1016/j.conbuildmat.2009.10.006.
[58] Marra, A. A., *Technology for Wood Bonding – Principles in Practice*, (Van Nostrand Reinhold Company, New York, 1992).
[59] Pocius, A. V., *Adhesion and Adhesives Technology: An Introduction*, 2nd ed., (Hanser Gardner Publications, Cincinnati, 2002).
[60] Pizzi, A. and Mittal, K. L. (Eds)., *Handbook of Adhesive Technology*, 2nd ed., (CRC Press, Boca Raton, Florida, 2003).
[61] Lyons, J. S. and Ahmed, M. R., *J. Reinforc. Plast. Compos.* **24**, 405–412 (2005).
[62] Corleto, C. R. and Bradley, W. L., *ASTM STP* **1012**, 201–221 (1989).
[63] O'Brien, T. K., *ASTM STP* **1330**, 3–18 (1998).
[64] Bao, F. C., Jiang, Z. H., Jiang, X. M., Lu, X. X., Luo, X. Q., and Zhang, S. Y., *Wood Sci. Technol.* **35**, 363–375 (2001).
[65] Downes, G. M., Hudson, I. L., Raymond, C. A., Dean, G. H., Michell, A. J., Schmileck, L. R., Evans, R., and Muneri, A., *Sampling Plantation Eucaliptus for Wood and Fibre Properties*, (CSIRO Publishing, Collingwood, 1997).